Neurochemical Research, Vol. 27, No. 10, October 2002 (© 2002), pp. 1113–1121

Statistical Analysis of Multiplex Brain Gene Expression Images

Alex Ossadtchi,[1] Vanessa M. Brown,[2,3] Arshad H. Khan,[2,3] Simon R. Cherry,[4] Thomas E. Nichols,[5] Richard M. Leahy,[1] and Desmond J. Smith[2,3,6]

(Accepted August 13, 2002)

Analysis of variance (ANOVA) was employed to investigate 9,000 gene expression patterns from brains of both normal mice and mice with a pharmacological model of Parkinson's disease (PD). The data set was obtained using voxelation, a method that allows high-throughput acquisition of 3D gene expression patterns through analysis of spatially registered voxels (cubes). This method produces multiple volumetric maps of gene expression analogous to the images reconstructed in biomedical imaging systems. The ANOVA model was compared to the results from singular value decomposition (SVD) by using the first 42 singular vectors of the data matrix, a number equal to the rank of the ANOVA model. The ANOVA was also compared to the results from non-parametric statistics. Lastly, images were obtained for a subset of genes that emerged from the ANOVA as significant. The results suggest that ANOVA will be a valuable framework for insights into the large number of gene expression patterns obtained from voxelation.

KEY WORDS: ANOVA; microarray; mouse; Parkinson's disease; singular value decomposition; voxelation.

INTRODUCTION

A genome-wide knowledge of gene expression patterns should help in understanding the molecular basis of the brain. Possible insights include the identification of gene expression "signatures" responsible for various brain regions as well as networks of co-regulated genes and their relevant control regions. Such networks can be compiled from co-ordinate spatial and temporal expression patterns emerging from variations due to anatomy, development, disease, environmental and genetic perturbations. In addition, extensive gene expression data sets should allow identification of genes induced and repressed in disorders affecting the brain.

To facilitate the ultimate goal of a comprehensive database of all brain gene expression patterns, a method called voxelation has been developed. Voxelation employs high-throughput gene expression analysis of spatially registered cubes (voxels) to produce volumetric expression maps for many genes in parallel. The voxel, from which the method is named, refers to an image volume element, the 3D analog of the pixel. The maps of gene expression produced by voxelation are analogous

[1] Department of Electrical Engineering, Signal and Image Processing Institute, School of Engineering, University of Southern California, Los Angeles, CA 90089.
[2] Department of Molecular and Medical Pharmacology, School of Medicine, University of California, Los Angeles, CA990095.
[3] Crump Institute for Molecular Imaging, School of Medicine, University of California, Los Angeles, CA 90095.
[4] Department of Biomedical Engineering, College of Engineering, University of California, Davis CA 95616.
[5] Department of Biostatistics, School of Public Health, University of Michigan, Ann Arbor, MI 48109.
[6] Address reprint request to: Desmond J. Smith, Department of Molecular and Medical Pharmacology, UCLA School of Medicine, 23-120 CHS, Box 951735, Los Angeles, CA 90095-1735. Tel: 310-206-0086; Fax: 310-825-6267; E-mail: DSmith@mednet.ucla.edu

0364-3190/02/1000–1113/0

to the images reconstructed in biomedical imaging systems, such as CT and PET. The method has been employed together with microarrays to investigate gene expression patterns in both human and mouse brains, normal and disordered (1–3).

In the mouse study, 40 voxel images for 9,000 genes were acquired from brains of both control mice and mice in which a pharmacological model of Parkinson's disease (PD) had been induced by methamphetamine (MA). The investigation uncovered networks of co-regulated genes common to both the normal and PD brain, allowing putative control regions responsible for these networks to be identified. In addition, genes involved in cell/cell interactions were found to show prominent regulation in the PD brain. Singular value decomposition (SVD), a mathematical method which provides parsimonious explanations of complex data sets, identified orthogonal gene vectors and their corresponding images that differentiated between normal and PD brain structures. Most pertinently, the third principal component was most strongly expressed in the striatum and cerebellum in the normal brain, suggesting a hitherto unsuspected genetic connection between these otherwise distinct brain regions. In contrast, the PD brain showed a shift of this principal component away from the striatum and cerebellum, towards the hippocampus. This dramatic change is consistent with the fact that the striatum is one of the brain regions most strongly affected in PD.

The above analyses used standard "discovery" tools geared towards mining understanding from large data sets. Recently, the use of ANOVA models has been advocated as a systematic approach to the design and analysis of microarray experiments (4–6). In this study, we employed ANOVA to analyze the data sets obtained from voxelation analysis of normal and MA treated mouse brains. We show that there is good agreement between the types of information obtained from discovery approaches such as SVD and model based approaches such as ANOVA. We also show that ANOVA models can efficiently explain much of the variance in data from voxelation studies.

EXPERIMENTAL PROCEDURE

Creation of PD Model. Adult C57BL/6J male mice (10 to 24 weeks, 25 to 31 g) received four i.p. injections of MA hydrochloride (10 mg kg^{-1} $injection^{-1}$ using 1.5 mg ml^{-1} solution) at 2-hour intervals (2,7,8). Mice were analyzed seven days after MA treatment. Induction of the PD phenotype was confirmed by demonstrating statistically significant decreases of dopamine and its metabolites dihydroxyphenylacetic acid and homovanillic acid in the striatum of MA treated mice (2). In addition, expression of tyrosine hydroxylase, the rate-limiting enzyme for biosynthesis of dopamine, was found to show statistically significant decreases in the substantia nigra. The specificity of changes in dopaminergic neurotransmission was shown by the lack of significant striatal changes in levels of 5-hydroxytryptamine (5-HT or serotonin), an independent neurotransmitter, and its metabolite 5-hdyroxyindoleacetic acid.

Voxelation of Mouse Brains. Mouse brains were voxelated as described (2). Briefly, brains were cut into superior and inferior halves, and divided into 10 coronal sections equally spaced by 1 mm. Each slice was then bisected down the midline, resulting in a total of 40 voxels, an average volumetric resolution of 7.5 μl. Registration employed the Mouse Brain Library (9,10). Voxelation was found to be essentially invariant between brains.

Microarray Analysis. Microarray analysis was performed as described (2). For each voxel, 100 μg of Cy3 labeled voxel RNA and 100 μg of Cy5 labeled control RNA were co-hybridized to a 9,000 gene microarray. The control RNA facilitated interarray comparisons, and consisted of total normal C57BL/6J mouse brain RNA. To obtain sufficient RNA (100 μg) for the microarray analysis, equivalent voxels of multiple brains were pooled. A total of 29 brains gave sufficient material, even for the smallest voxels (slice 1, most anterior). The microarrays contained 9,000 spots, some of which represented controls or replicates, and consequently there was a total of 8,137 unique genes. Normalization was performed as described (2).

ANOVA. ANOVA was performed as described (4–6). Briefly, the study followed a reference design experiment, where the total brain RNA (Cy5) was the reference sample, and the voxel RNA (Cy3) was the experimental. Effects were defined as variety (±MA), slice (S), superior-inferior (P), and hemisphere (H). The prevalence of effects across genes was measured as the proportion of genes with an F-statistic greater than 4; if there is no significant effect approximately 5% of the genes should have such an F-value. Use of uncorrected thresholds does not control for false positives due to multiple comparisons. We use these thresholds not to make inference on individual genes, but rather as a screening device which will minimize Type II errors and identify genes worthy of further study.

Nonparametric Analysis. A permutation (Monte-Carlo) method was employed for non-parametric analysis (11). To examine each effect and ensure exactness of the test, a proper realignment was chosen such that the F-statistics of interest had the largest value (maximally affected by the permutations performed). Since for some effects the number of possible permutations is extremely large, the Monte-Carlo scheme was used for random and uniform sampling of the permutations.

RESULTS

ANOVA Model. The model is based on:

$$R_g = \log_2\left(\frac{I_g^{Cy3}}{I_g^{Cy5}}\right) \qquad (1)$$

where: R_g is normalized log gene expression ratio for gene g, I_g^{Cy3} is normalized intensity in Cy3 channel, and I_g^{Cy5} is normalized intensity in Cy5 channel.

Table I. ANOVA Model

	μ	V	S	P	H	SP	SH	SV	VP	VH	Total	Available
df[a]	1	1	9	1	1	9	9	9	1	1	42	80
Columns[b]	1	2	3–11	12	13	14–22	23–31	32–40	41	42	—	—
%F > 4[c]	—	52.3	21.6	12.2	11.1	1.6	1.01	12.0	6.6	13.4	—	—
SV corr.[d]	0.98	0.98	0.83	0.89	0.8	0.73	0.68	0.8	0.73	0.78		

[a] Degrees of freedom.
[b] c.f. Fig. 1.
[c] Percentage of genes with F-ratio > 4. In case of parametric analysis, this would correspond to significance level of 5%.
[d] Singular vector correlation coefficients. This row shows for each effect the correlation coefficients between the subspaces spanned by the corresponding columns of the design matrix and the first 42 singular vectors of the data matrix.

The following model was employed, as described (4–6):

$$r_{ijkl} = \mu + V_i + S_j + P_k + H_l + SP_{jk} + SH_{il} + SV_{ji} + VP_{ik} + VH_{il} + \varepsilon_{ijkl} \quad (2)$$

where μ is grand mean, V_i is variety effect (±MA), $i = \{1,2\}$, S_j is slice effect, $j = \{1,2,3 \cdots 10\}$, P_k is superior vs. inferior effect, $k = \{1,2\}$, H_l is left vs. right hemisphere effect; $l = \{1,2\}$, SP_{jk} is slice-(sup-inf) interaction, SH_{il} is slice-hemisphere interaction, SV_{ji} is slice variety interaction, VP_{ik} is variety-(sup-inf) interaction VH_{il} is variety-hemisphere interaction, ε_{ijkl} is error.

Note that this model uniquely specifies each voxel by virtue of slice, hemisphere, and superior-inferior indices. Also note that by fitting each gene independently, we effectively fit an interaction of the genes with all of the effects delineated in the model. The degrees of freedom are shown in Table I. There is a total of 80 degrees of freedom, and 42 of these are employed in the model. Assuming that observations are missing at random, then absent values are easily accommodated by deleting the corresponding row of the design matrix (12). It is only necessary to check that the effects are estimable, that is, the design matrix is of full rank. A total of 38 degrees of freedom (80 minus 42) remain to estimate error. However, since there are no replications, the error is aliased (indistinguishable) from all 3-way interactions and the one 4-way interaction. The presence of redundant degrees of freedom is an important observation, because failure to meet quality control standards means that a large number of genes have less than 80 measurements (40 voxels for both the +MA and −MA brains). For example, provided a gene has less than 18 bad spots, there will still be more than 20 degrees of freedom to estimate the residual variance. The design and aliasing matrices resulting from the model are shown in Figure 1. A total of 497 genes out of 8,137 unique genes on the microarray had measurements that exceeded quality control standards for all

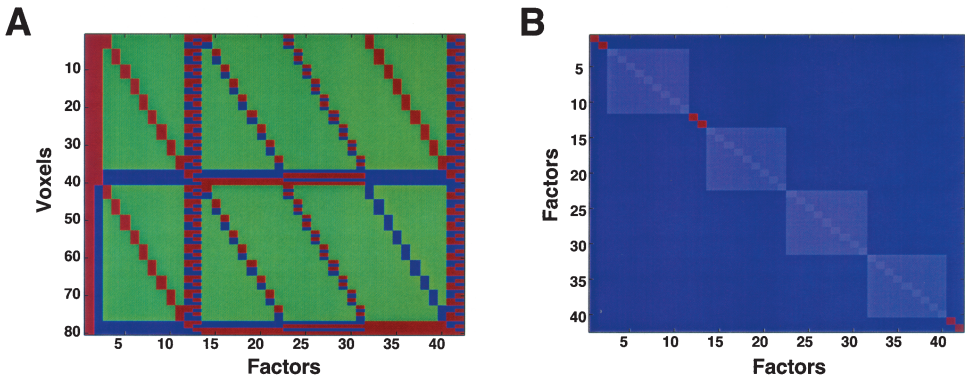

Fig. 1. Design and information (aliasing) matrices. (**A**) Design matrix. The rows of the matrix represent the 80 voxels analyzed in the study, with rows 1–40 representing the control brains and rows 41–80 representing the MA treated brains. The voxel numbering proceeds from anterior to posterior in the rows of the matrix, such that voxels A1, A2, A3... ...I2, I3, I4 of the normal brain (2) correspond to rows 1, 2, 3... ...37, 38, 39, 40, respectively. The columns of the matrix correspond to the factors of the ANOVA (Table I). Red = 1, green = 0, blue = −1. (**B**) Information or aliasing matrix. The proposed model corresponds to a balanced orthogonal design, allowing for unconfounded estimates of the factors. Dark blue = 0, light blue = 16, red = 80.

80 voxels. These 497 genes are employed in one of the analyses described below.

Results of ANOVA Model. The ANOVA model was applied to all 8,137 genes, and found to explain 80% of the variance. The results for each of the 9 effects (excluding grand mean) of the ANOVA model (four main: V, S, P, H; five two-way interactions: SP, SH, SV, VP, VH) are displayed in Table I. The table shows the proportion of genes out of the 8,137 analyzed where the F-statistic is >4. Of the main effects (V, S, P, and H), the effect showing the largest contribution is the variety effect (V, or $\pm$MA) (4,255 genes out of 8,137, or 52.3%), followed by slice (S) (21.6%), variety-hemisphere (VH) interaction (13.4%), and sup-inf effects (P) (12.2%). It is not surprising that the sup-inf effects (P) make a smaller contribution to explaining the variance than the first two main effects (V and S), since many major brain structures (e.g., cortex, hippocampus) are shared between the superior and inferior halves of the brain. As expected, the hemisphere effect (H) makes the smallest contribution among the main effects (895 genes), since the mouse brain shows a high degree of bilateral symmetry.

Of the two-way interactions, perhaps not surprisingly, the slice-variety (SV) interaction had high explanatory power, second after variety-hemisphere (VH) interaction. Much of the relatively high value of the VH interaction can be attributed to the confounding effect of genes with less than 80 good measurements. When ANOVA analysis is run on the set of 497 genes with all 80 measurements, the proportion of genes with high VH effect (significance level of 5%) drops to 7.1%. This is an example of the fact that ANOVA allows for reasonable handling of missing values. During the estimation step, rows of the design matrix corresponding to the missing values can be removed. The modified matrix no longer corresponds to a balanced design, but still permits unbiased estimates for the effects, assuming that observations are missing at random. Figure 2 shows the F-ratios for all effects based on the 497 genes with 80 measurements. This plot is useful in identifying "interesting" genes for the various effects.

Comparison of ANOVA and SVD. SVD is a discovery tool for analysis of large data sets (13–15). The method maintains the maximum possible fraction of the variance from the original data, while reducing dimensionality. SVD does not rely on pre-specified hypotheses, and is entirely data driven. In contrast, ANOVA relies on hypothetical models to explain the structure of

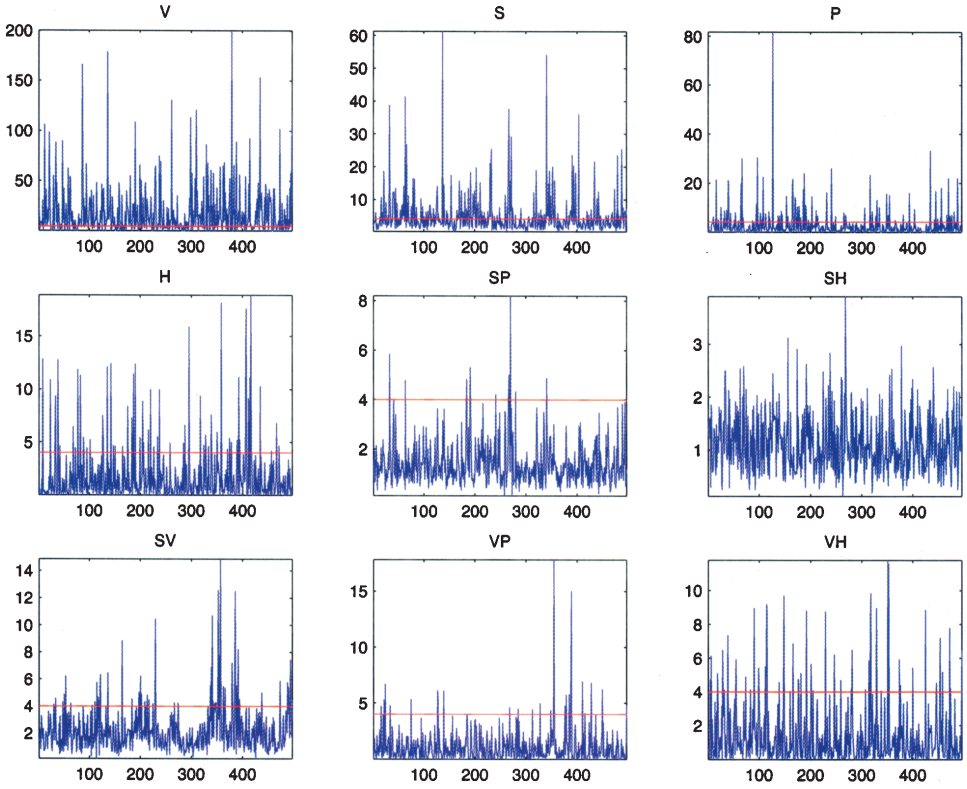

Fig. 2. F-statistics for different effects. For clarity, only genes with all 80 measurements (497 genes) are shown on the plots. The red lines correspond to the value of 4, which is roughly equivalent to $p = 0.05$ for the distributions F(1,38) and F(9,38).

data. We compared the ANOVA analysis with SVD (2), by using correlation metrics of each ANOVA effect in the subspaces spanned by the corresponding columns of the design matrix and the first 42 singular vectors of the data matrix (Table I, last row). It can be seen that not even all main effects are well captured by the first singular vectors of the data matrix. Thus, the V effect is captured by SVD, whereas variance explained by most of the other effects is partitioned into the SVD noise space. This suggests that SVD should be used with care when processing noisy data, where effects of potential interest may not be predominant in power. Nevertheless, if proper care is exercised our results show that SVD can be used as a tool to decrease noise, without the necessity of building a specific model.

Comparison of Parametric and Nonparametric Approaches for Estimation of P-Values. To further compare parametric (ANOVA) and non-parametric approaches, we used a permutation (Monte-Carlo) method for the non-parametric analysis (11). The results of the investigation are shown in Figure 3, where by means of Q-Q plots, parametric and non-parametric permutation distributions are compared for the main effects using F-statistics. Of the main effects, the hemisphere (H) and sup-inf (P) effects had the least significant F-statistics (Table I), and hence, as expected, the p-values obtained using ANOVA are very similar to those obtained using the permutation method (Fig. 3). In contrast, the variety (V) and slice (S) effects had the most significant F-statistics (Table I) and showed a marked divergence between the ANOVA p-values and the non-parametric p-values (Fig. 3). The main reason for using non-parametric statistics is the presence of noticeable non-normality in residual errors. However, permutation testing of ANOVA models is complicated when both main effects and interactions are present. The tests of main effects must be performed in a way that are valid regardless of interaction effects. This complex issue involves concepts related to realignment, and is a subject for future research.

Imaging. In order to map gene expression patterns, we focused on genes from the intersection of two sets (Fig. 4). The first set was comprised of those genes with a significant SV effect ($p < 0.05$), and the second set consisted of those genes consistently expressed in the two hemispheres ($p > 0.1$). A total of 588 genes resulted

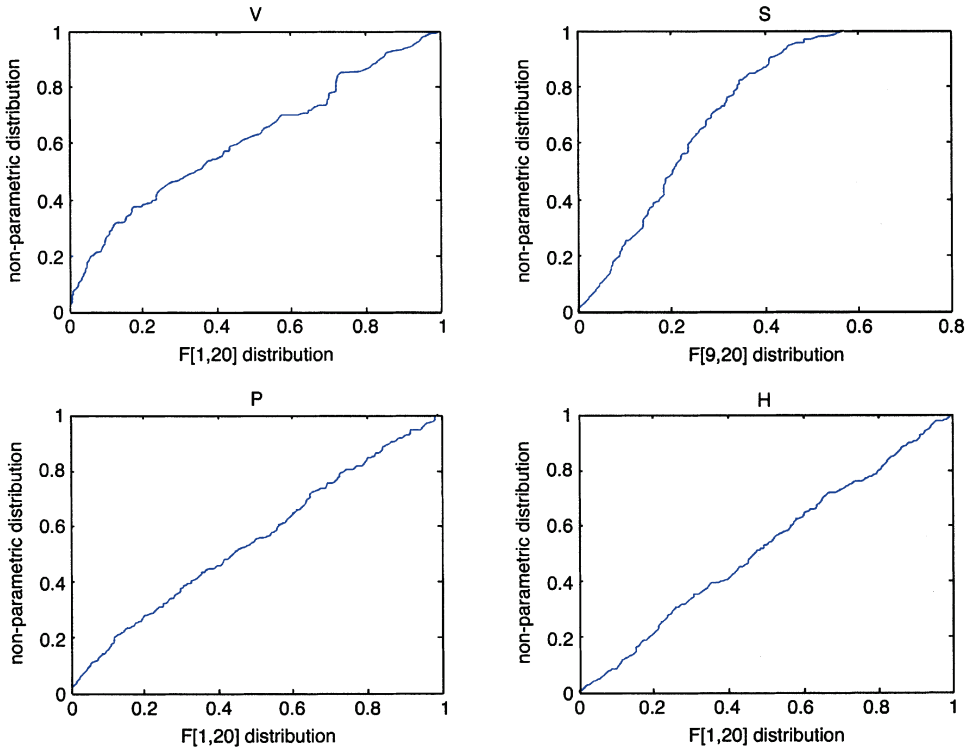

Fig. 3. Q-Q plots for comparison of parametric and non-parametric p-values. Identical distributions would correspond to a straight line of the form $y = x$. Differences between parametric and non-parametric (permutation) distributions can be attributed to both non-normality of the residuals as well as confounds with higher order effects in the permutation test.

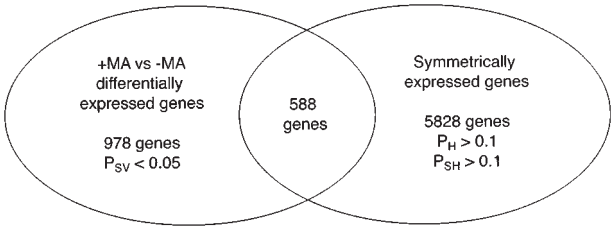

Fig. 4. Selecting genes for spatial expression profiles. Named genes in the selected 588 gene intersection are listed in Table II.

from this procedure, and the named genes in the intersection are shown in Table II. The profiles of all 588 genes for the slice-variety (SV) interaction effect are shown in Figure 5. The profiles have been sorted into clusters on the basis of a nearest-neighbor similarity metric (1,2). A total of ten clusters emerged from the sorting. It can be seen that there are several slices most responsible for the differences between −MA and +MA mice. Most prominent amongst these is slice 9, which is contained within the cerebellum. This uncovered difference between the brains is similar to that identified using very different analytic approaches (2). A graphic representation (2) of the spatial expression pattern for one of the genes in cluster 5, *Nfl* (neurofilament light chain gene) is shown in Figure 6A. There were two different spots (clones) corresponding to the Nfl gene on the microarrays, providing an opportunity to assess within-array replicability. As seen in Fig. 6A, there was excellent within-array reproducibility for both the −MA and the +MA brains. Fig. 6B provides a graphic representation of the spatial expression pattern for a gene from cluster 9, *Man2a1* (mannosyl-oligosaccharide 1,3-1,6-alpha-mannosidase gene) (EC 3.2.1.114) in the −MA and +MA brains.

DISCUSSION

Voxelation results in large data sets, over 700,000 for the Parkinson's disease model discussed here. Nevertheless, an important future goal for voxelation will

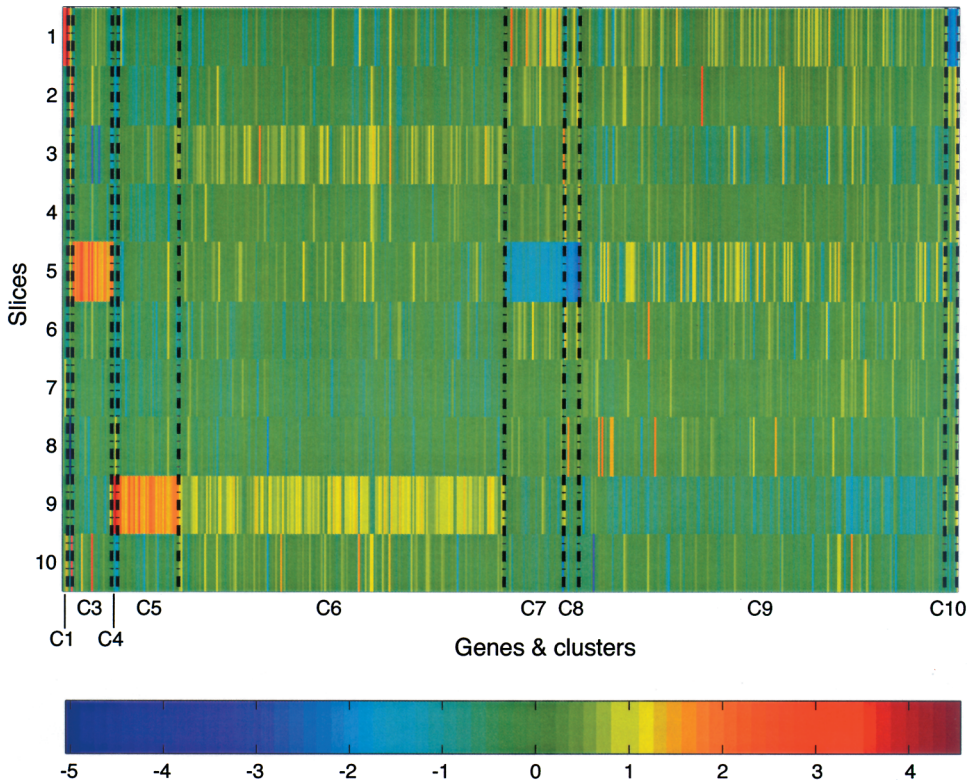

Fig. 5. Clustered SV (slice-variety) effect profiles for the 588 selected genes (Fig. 4). The plot indicates the slices contributing to the differential expression between +MA and −MA brains. The rows of the matrix represent the 10 slices analyzed in the study (slice 1, anterior; slice 10, posterior). The value of SV effect for a gene in any slice is read by looking along the relevant row and column, finding the intersection, and referring to the scale. Blue indicates +MA > −MA and red indicates −MA > +MA. Gene clusters are indicated along the bottom of the plot (e.g. C4). The gene clusters showing a strong divergence between −MA and +MA brains in slice 9 are in agreement with previous work (2). In addition, several new clusters are revealed.

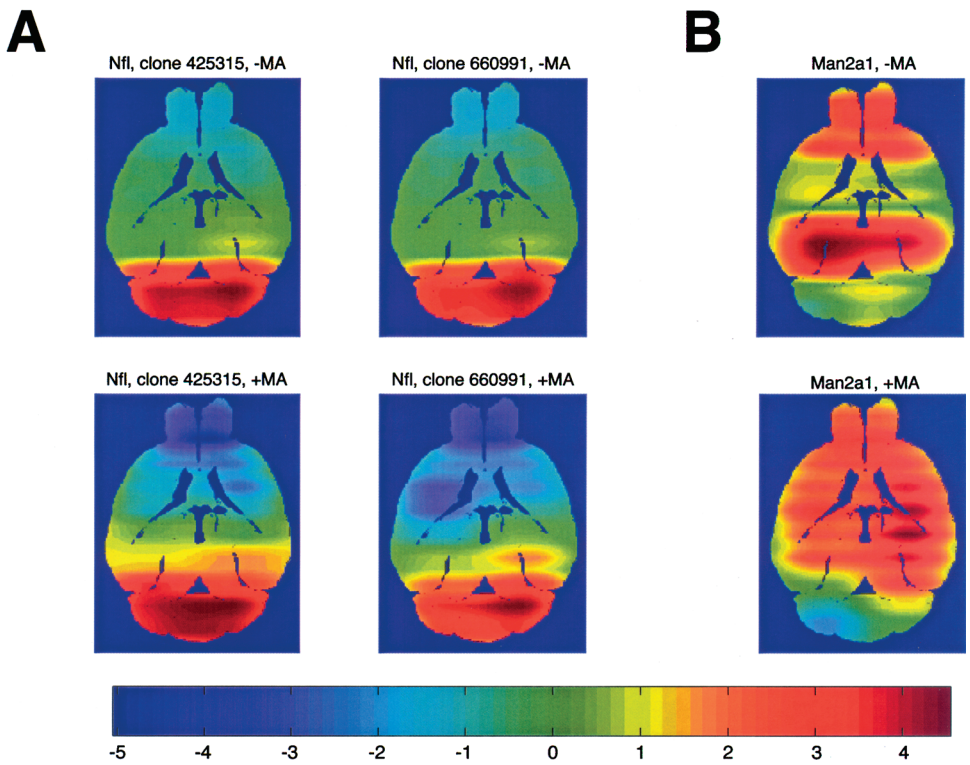

Fig. 6. Spatial expression patterns. (**A**) Expression pattern of the *Nfl* gene (cluster 5) as judged from two separate spots (clones) on the microarrays. The expression patterns of the gene in the normal (top row) and MA brain (bottom row) are presented using a midlevel transverse section corresponding to section 8 of the Mouse Brain Library (interaural 5.40 mm, bregma −4.60 mm) (2,9,10). Imaging software smoothed the expression patterns over voxels. The level of gene expression can be deduced by reference to the pseudocolor scale. The plot demonstrates excellent within-array reproducibility (r for −MA brain = 0.96, $F(1,38) = 443.65$, $p < 0.0001$; r for +MA brain = 0.90, $F(1,38) = 153.80$, $p < 0.0001$). (**B**) Differential expression of the *Man2a1* gene (cluster 9) in the −MA and +MA brains.

be to increase the amount of information it produces, both by decreasing voxel size to improve spatial resolution, and also by analysis of larger numbers of genes. These objectives will require advances in miniaturization to allow spatially registered harvesting of the smaller voxels, and automation to allow greater speed in processing the increased numbers of voxels and genes. Such objectives will provide substantial engineering challenges, but the success of the genome project provides a paradigm for implementation of such a program. Consequently, it is likely that the data sets from future voxelation projects will become extremely large. For example, a 325,000 voxel reconstruction of the human brain for all 30,000 genes will result in a data set of 10^{10} (3). Such immense data sets will require careful statistical evaluation.

In this study, we used an ANOVA model (4–6) to provide a framework for statistical analysis of gene expression data from control brains and brains from a model of PD. Of the main effects, the variety (V, or ±MA), slice (S) and sup-inf (P) effects explained the largest part of the variance, while the hemisphere effects explained least. Comparison of the ANOVA model and that suggested by SVD showed reasonable agreement. However, the SVD was less sensitive in detecting weak effects, as would be expected for a non-parametric discovery method. There was good agreement between ANOVA (parametric) and permutation (non-parametric) approaches for the two weakest main effects (hemisphere and sup-inf). Perhaps surprisingly, however, for the two strongest main effects (variety or ±MA and slice), there appeared to be a striking deviation between the parametric and non-parametric approaches. When a subset of genes with significant variety-slice (VS) interaction and consistent expression between the hemispheres was examined, the greatest difference in spatial gene expression patterns between the control and MA brains appeared to be in slice 9, part of the cerebellum. This strongly agrees with previous findings obtained using distinct analytical tools (2).

Table II. Gene Clusters[a]

Cluster	Gene name	Clone ID	Cluster	Gene name	Clone ID	Cluster	Gene name	Clone ID
1	Ldlb	457892	6	Macs	618661	8	Lama4	736616
	Psmb3	571569		Mad4	846536	9	Atp1b1	493488
2	Col6a3	480620		Mbc2	575700		Atp2a1	318735
3	Meox1	419684		Mbd2	421592		Bach2	640200
	Pkd2	455813		Mbp	480753		Bckdk	480575
4	Cals1	692913		Mea1	484122		Bhmt	423156
	D0H4S114	733420		Mem3	775464		Bmp1	466306
	Mdk	671218		Mkln1	676111		Cast	577089
5	Agt	733572		Msf	352302		Cd6	637369
	Akt	678740		Mt1	480068		Cirbp	475679
	Btf3	692936		Ndufv1	864576		Col5a1	425344
	D3Wsu133e	889470		Nte-pending	352795		Cyp2c40	583799
	Ndr3	677163		Pdgfra	735605		Dok2	438282
	Nfl	660991		Per	949546		Es2el	318785
	Nfl	425315		Plaa	831959		Es31	719734
	Pnutt2	889281		Plunc	472623		Falm-pending	351720
	Rab7	779604		Pmp20-pending	437209		Galgt1	637290
	Rpl3	570533		Ppp2r1a	733882		Gll1	640751
	Tstap35b	660586		Proc	692609		Gpx3	551164
	Tuba4	329726		Prpk	876060		Gpx3	577594
				Psma1	723267		Gstz1	672972
	Tubb4	671340		Ptpn16	575665		Gtr2	388376
	Vbp1	693287		Pttg1	678793		Habp2	748390
	Vdac3	680191		Rab11b	659369		Hck	638455
6	Abca2	850420		Rac2	891108		Hrsp12	676532
	Aco1	677092		Rpl7	524442		Hs6st1	736858
	Acox-pending	747880		Rpo2-4	636513		lfi1	651927
	Adam17	385467		Rps12	577267		ll12b	720765
	Anxa6	876698		S100a1	872869		lrf2	639197
	Anxa7	681168		Selpl	876033		ltlh1	734289
	Bhmt	680854		Silg81	476180		ltm2b	481400
	Car2	579391		Srp54	597566		Jak2	621226
	Crya2	672201		Stau1	576918		Kap	579721
	Ctbp1	677093		Stk11	933770		Kifc1	426992
	Cugbp2	597832		Sul1-rs1	888602		Klk8	483813
	Cugbp2	620221		Surf4	695279		Ltf	874383
	D17H6S45	421962		Timm17a	318134		Lum	746644
	D19Wsu55e	672881		Timp2	831964		Madh3	456861
	D7Wsu87e	679464		Tle3	722501		Man2a1	315962
	D8Wsu49e	920414		Ttc3	775150		Myb	721803
	ESTM2	355356		Ubce7	482359		Nfkbla	641058
	Fgd1	733780		Ube3a	721372		Nr1h4	748622
	Gbas	333579		Ubp1	949534		Pdlr	873690
	Gdm1	351221		Uchl1	763647		Pola2	476123
	Ggh	733456		Zfp238	472595		Rab25	697383
	Glns	440344		Uchl1	763647		S100a11	669969
	Gys3	660012		Zfp238	472595		Spry1	425005
	Hdac1	374877	7	Adam22	418732		Supt4h	749558
	Hsc70	573857		Gbp2	583808		Tead2	388244
	lna	660756		lfj203	618572		Tmpo	597352
	ltm2b	720342		Sec61a	37384		Twist	331264
	Klf9	874192		Stc	474298		Tyrobp	671865
	Krt2-1	476999		Tfg	316835		U2af1-rs1	747294
	Lorsdh	738285		Twist	479367	10	Masp2	680232
	Ly6	580715	8	Cdc2a	468792			

[a]Named genes of the selected 588 genes (Fig. 4). Genes are alphabetically ordered within each cluster.

Additional strategies can be envisaged for interrogation of voxelation data sets. Gene shaving (16) identifies subsets of co-regulated genes with large variations across conditions (voxels). This approach is distinguished from hierarchical clustering and other commonly used methods by the characteristic that genes may belong to more than one cluster. Moreover, the clustering can be supervised by an outcome measure. Another approach to extracting insights could employ stratification of the data (e.g., Table I) into classes of genes on the basis of function using the Gene Ontology Database (17).

The spatial information from voxelation can be used with advantage by considering the slice (S) effect as ordered, analogous to a time course. For example, the full-arbitrary parameterization of the slice effect could be replaced with a linear gradient or low-order (orthogonal) polynomial parameterization. In this way, incorporating prior information from spatial contiguity or slice/gradient effects would allow the use of more sophisticated ANCOVA models, which might dramatically increase statistical power as well as providing improved visualization possibilities.

The ANOVA and SVD were compared by looking at the correlation of the SVD vectors with columns of the design matrix (Table I). An alternative approach would be to perform SVD on a sub-data matrix consisting exclusively of those genes which show selected interaction effects. It might also be useful to find the correlations of the SVD vectors with relevant linear contrasts, which in essence represent a rotation of the design matrix (Fig. 1). For example, a set of contrasts could be created for the variety effect to build up a voxel; each one of the contrasts would correspond to a single voxel.

The ANOVA allowed reasonable handling of missing values, but additional strategies could be employed. Multiple imputation replaces each missing data point with plausible values (18), and the completed data sets are analyzed using standard statistical approaches. This allows recovery of parameter estimates and standard errors which take into account the uncertainty due to missing values.

In summary, the present study suggests that ANOVA will provide a useful framework for analysis of multiplex brain gene expression data sets. In addition, ANOVA showed good agreement with SVD, but somewhat higher sensitivity. These findings indicate that future analysis of voxelation data sets may benefit from a combined attack using both ANOVA models and discovery methods such as SVD.

ACKNOWLEDGMENTS

Supported by grants from the Dana Foundation, Merck Genome Research Institute, Staglin Music Festival and NARSAD Young Investigator Award, W. M. Keck Foundation, National Foundation for Functional Brain Imaging, NIH (NS39628, DA015802), NSF (DB1-0079375), and UCLA School of Medicine.

REFERENCES

1. Brown, V. M., Ossadtchi, A., Khan, A. H., Cherry, S. R., Leahy, R. M., and Smith, D. J. 2002. High-throughput imaging of brain gene expression. Genome Res. 12:244–254.
2. Brown, V. M., Ossadtchi, A., Khan, A. H., Yee, S., Lacan, G., Melega, W. P., Cherry, S. R., Leahy, R. M., and Smith, D. J. 2002. Multiplex three dimensional brain gene expression mapping in a mouse model of Parkinson's disease. Genome Res. 12:868–884.
3. Peterson, A. S. 2002. Pixelating the brain. Genome Res. 12: 217–218.
4. Kerr, M. K., Martin, M., and Churchill, G. A. 2000. Analysis of variance for gene expression microarray data. J. Comput. Biol. 7:819–837.
5. Kerr, M. K. and Churchill, G. A. 2001. Statistical design and the analysis of gene expression microarray data. Genet. Res. 77: 123–128.
6. Kerr, M. K. and Churchill, G. A. 2001. Experimental design for gene expression microarrays. Biostatistics 2:183–201.
7. Sonsalla, P. K., Jochnowitz, N. D., Zeevalk, G. D., Oostveen, J. A., and Hall, E. D. 1996. Treatment of mice with methamphetamine produces cell loss in the substantia nigra. Brain Res. 738:172–175.
8. Melega, W. P., Raleigh, M. J., Stout, D. B., Lacan, G., Huang, S. C., and Phelps, M. E. 1997. Recovery of striatal dopamine function after acute amphetamine- and methamphetamine-induced neurotoxicity in the vervet monkey. Brain Res. 766:113–120.
9. Williams, R. W. 2000. Mapping genes that modulate mouse brain development: a quantitative genetic approach. Pages 21–49, *in* Goffinet, A. F., and Rakic, P. (eds.), Mouse Brain Development, Springer, New York.
10. Rosen, G. D., Williams, A. G., Capra, J. A., Connolly, M. T., Cruz, B., Lu, L., Airey, D. C., Kulkarni, K., and Williams, R. W. 2000. The Mouse Brain Library @ www.mbl.org. Int. Mouse Genome Conf. 14:166. www.mbl.org.
11. Nichols, T. E. and Holmes, A. P. 2002. Nonparametric permutation tests for functional neuroimaging: a primer with examples. Hum. Brain Mapp. 15:1–25.
12. Little, R. J. A. and Rubin, D. B. 1987. Statistical Analysis with Missing Data, John Wiley & Sons, New York, NY.
13. Alter, O., Brown, P. O., and Botstein, D. 2000. Singular value decomposition for genome-wide expression data processing and modeling. Proc. Natl. Acad. Sci. USA 97:10101–10106.
14. Frackowiak, R. S. J., Friston, K. J., Frith, C. D., Dolan, R. J., and Mazziotta, J. C. 1997. Human Brain Function, Academic Press Ltd., London, UK.
15. Hendler, R. W. and Shrager, R. I. 1994. Deconvolutions based on singular value decomposition and the pseudoinverse: a guide for beginners. J. Biochem. Biophys. Methods 28:1–33.
16. Hastie, T., Tibshirani, R., Eisen, M. B., Alizadeh, A., Levy, R., Staudt, L., Chan, W. C., Botstein, D., and Brown, P. 2000. 'Gene shaving' as a method for identifying distinct sets of genes with similar expression patterns. Genome Biol.
17. Gene Ontology Consortium. http://www.geneontology.org/.
18. Sinharay, S., Stern, H. S., and Russell, D. 2001. The use of multiple imputation for the analysis of missing data. Psychol. Methods 6:317–329.